



# Hydric Cycle Impacts on CO<sub>x</sub> Argillite Permeability and Young's Modulus

Zhibo Duan<sup>1,2,3</sup> · Frédéric Skoczylas<sup>1,2,3</sup> · Chuanrui Wang<sup>3</sup> · Jean Talandier<sup>4</sup>

Received: 17 February 2020 / Accepted: 19 September 2020 / Published online: 8 October 2020  
© Springer-Verlag GmbH Austria, part of Springer Nature 2020

## Abstract

Wetting–drying cycles are likely to induce damage of claystone. To evaluate and to prevent micro-cracking impacts on Callovo-Oxfordian (CO<sub>x</sub>) argillite, which is, in France, the potential host rock of structures containing nuclear wastes, 18 months of tests were carried out on different series of samples. These tests consisted of gas permeability and Young's modulus measurements. They were carried out on dry material, as a reference state, previously submitted to successive cycles of wetting–drying. The results show without any ambiguity that repeated hydric cycles lead to damage i.e. additional micro-cracking that induces an increase in gas permeability (possibly by 2–3 orders of magnitude compared with the intact one) and decrease in Young's modulus by 5–15%. This means that strong precautions have to be followed to keep stable the initial material water content prior to the tests and to study a material representative of its in-situ state.

**Keywords** Argillite · Relative humidity (RH) · Wetting–drying cycles · Gas permeability · Young's modulus

## 1 Introduction

ANDRA (French agency for nuclear waste storage) is in charge in France for the management of the nuclear wastes. They have long been produced by 58 nuclear power reactors and other activities (medical, industrial, etc.). Claystone is expected to be a convenient natural barrier for long-term and high-level nuclear waste geological storage, thanks to its low initial permeability and high stability. An underground research laboratory has been designed at Bure site in the east of France. This laboratory is likely to become the official waste depository and it is hosted at great depth (400–500 m) in a clayed rock (CO<sub>x</sub> Argillite) that has many

required general properties such as low gas and water permeability, healing and sealing abilities, etc.

Based on this industrial context, various investigations have been carried out to investigate the mechanical and fluid transport properties of this argillite. A widely recognized view is that this clay rock is a transversely isotropic material and many experimental studies were carried out at different levels of water content (mechanical properties and permeability tests) on CO<sub>x</sub> and Opalinus Clay (OPA) clay-rich rock to confirm this point of view (Zhang and Rothfuchs 2004; Davy et al. 2007; Yang et al. 2013; Favero et al. 2018; Crisci et al. 2019). Compared to other typical sedimentary rocks, water content is a paramount parameter which highly affects the mechanical properties due to the particular water absorption characteristics and water-induced strength degradation effect (Zhang et al. 2014; Wild et al. 2015, 2017; Amann et al. 2017). Hence it is of great importance to identify the anisotropic deformation behavior (swelling and shrinkage) of argillaceous rock equilibrium at various relative humidity. Numerous authors (Rutqvist et al. 2001; Yang et al. 2012, 2013; Wang et al. 2015; Zieffle et al. 2017) carried out different methods to experimentally and numerically study the anisotropic mechanical property of argillite at various RH and mechanical loading. They often focused on micro-structure and micro-cracks occurrence during hydration and drying cycles (Freissmuth 2002; Valès 2008). As for the

✉ Frédéric Skoczylas  
frederic.skoczylas@centralelille.fr

<sup>1</sup> School of Civil Engineering, Architecture and Environment, Hubei University of Technology, Wuhan 430068, China

<sup>2</sup> Laboratoire de Mécanique, Multiphysique, Multiéchelle (LaMcube) UMR CNRS 9013, Avenue Paul Langevin, Cité scientifique, 59655 Villeneuve-d'Ascq Cedex, France

<sup>3</sup> Centrale Lille, Cité scientifique, CS20048, 59651 Villeneuve-d'Ascq Cedex, France

<sup>4</sup> Département Recherche and Développement, Service Mécanique des Fluides et des Solides, ANDRA, 1-7, rue Jean Monnet, 92298 Châtenay-Malabry, France

transport properties, researchers have executed extensive research on gas migration through intact and macro-cracked COx argillite (Patriarche et al. 2004; Davy et al. 2007, 2009) to assess the leak of the radionuclide at in-situ conditions. Especially for the fully saturated argillite (already swollen), it is validated that gas flows through the pores, filled with water, due to dissolution and diffusion phenomena (Marshall et al. 2005; Davy et al. 2013).

As a consequence, numerous studies on argillite have been performed by many French and European laboratories. The in-situ rock is submitted to a confining stress (around 12 MPa) and is fully water saturated. Hence, to be studied, this rock must undergo different steps such as unconfinement and modifications of its surrounding (temperature, hydric conditions, oxidation, etc.). This study mainly focused on the hydric problem as most of the laboratory tests performed for ANDRA are carried out on samples that have necessarily suffered from hydric changes (compared to the in-situ situation). It is crucial to evaluate how this fact can lead to deep modification as regards 'intact' material. This was the main goal of this long (18 months) study to underline that experimental conditions (or/and lack of precaution) are able to produce major changes of two (basic) properties: gas permeability and Young's modulus. As these changes can be attributed to the occurrence of cracking, hydric cycles are also likely to produce diffusion and thermal dilation property modifications (if the crack volume is significant).

## 2 Material

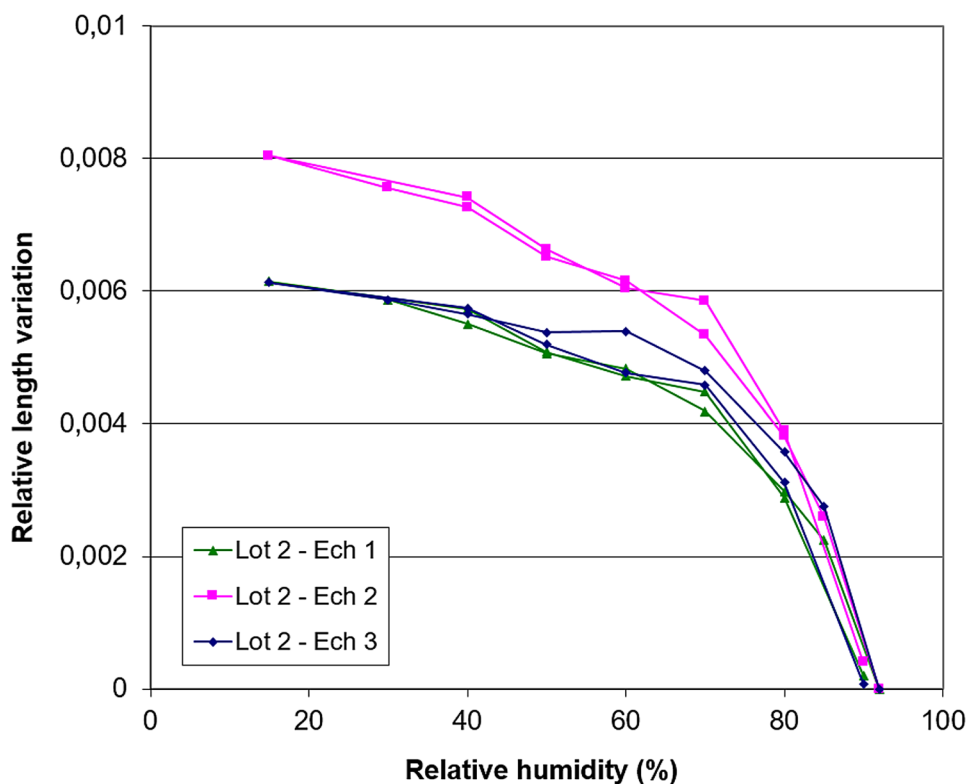
The argillite studied in our works is from the Callovo-Oxfordian (COx) argillaceous rock of the Meuse-Haute Marne in France. It is mainly composed of a clay matrix, quartz and carbonate. The average proportions of these components are approximately:  $45 \pm 7\%$  clay matrix,  $23 \pm 4\%$  quartz,  $27 \pm 9\%$  carbonate (calcite) and 5% feldspars, pyrite, and iron oxides (Zhang 2014).

## 3 Experimental Methodology

### 3.1 Damage Origin Related to Relative Humidity (RH) Change

The first question that arises about damage induced by relative humidity cycles is about the physical phenomena involved. Is it due to relative humidity variation itself or to the structural effect associated with this variation? It is well known that drying will bring about suction and shrinkage, which can be linked to significant strains (see Fig. 1). These results (obtained in our laboratory) show that, for argillite, a change from 90 to 10% (quasi dry state) in relative humidity can lead to strains as large as  $8000 \mu\text{m}/\text{m}$ . In the case of shrinkage prevented by structural effect, such (constrained)

**Fig. 1** Shrinkage observed for argillite samples



strains are able to produce tensile stresses and resulting cracking (Peron et al. 2009).

Drying (or wetting) is a very long process to achieve final equilibrium as for a large part the latter comes from vapor diffusion inside the sample. As an example, Fig. 2 plots mass variation v.s. time for small samples (10 mm diameter and 20 mm long) submitted to drying followed by wetting. Despite the small sample size, one can observe that several weeks are sometimes necessary to reach a stable mass. On the other hand, a decrease (or increase) in RH level leads to a rapid (2–3 days) decrease (or increase) in mass for these small size samples. Following this fast change, the sample mass is already close to the stable one, which needs much more time to be obtained. These results (obtained in LaM-cube laboratory) were used to choose the adequate sample dimensions to ensure a good compromise between experimental time and result quality (or reliability).

Experiments with high RH level on argillite sometimes lead to strong (localized) damage when pyrite (iron sulphur) is present inside the sample. The damage is then induced by a large pyrite swelling, which generally leads to a complete sample rupture. This kind of samples had been removed as they could not be tested.

As prevented shrinkage can lead to large tensile stress able to develop the material cracking. This issue can occur at different scales in the present case, a local scale if the material is heterogeneous (i.e. shrinkage of clay phase surrounding rigid inclusion) and a global scale (i.e. the sample size), which develops between drying and non-drying zones during the first steps of drying (i.e. before mass equilibrium

state). This is illustrated in Fig. 3 for the two kinds of the sample used for this study: 37 mm diameter and 10 mm thickness samples (37–10 in the following) for gas permeability tests and 20 mm diameter and 40 mm length (20–40 in the following) for Young modulus measurements. These size choices result from the necessary compromise mentioned before. For such dimensions, argillite can be considered as homogeneous. 37–10 samples are supposed to be adequate for gas permeability measurements and this technic had long shown its ability to detect cracking, especially when associated with confining pressure variations. Many causes are able to induce damage. It has, therefore, been chosen to favor the structural ones, occurring at the sample scale, as they are likely to be more detectable than the local ones

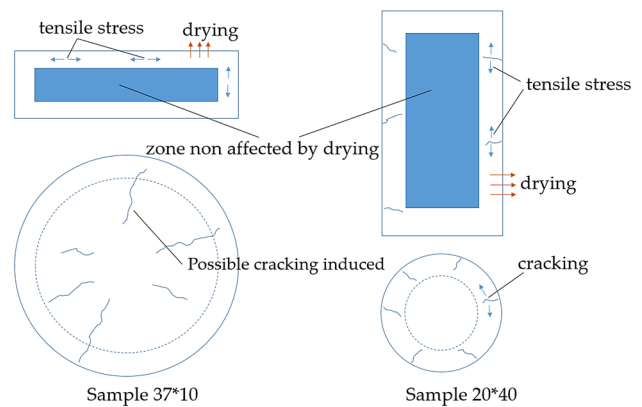
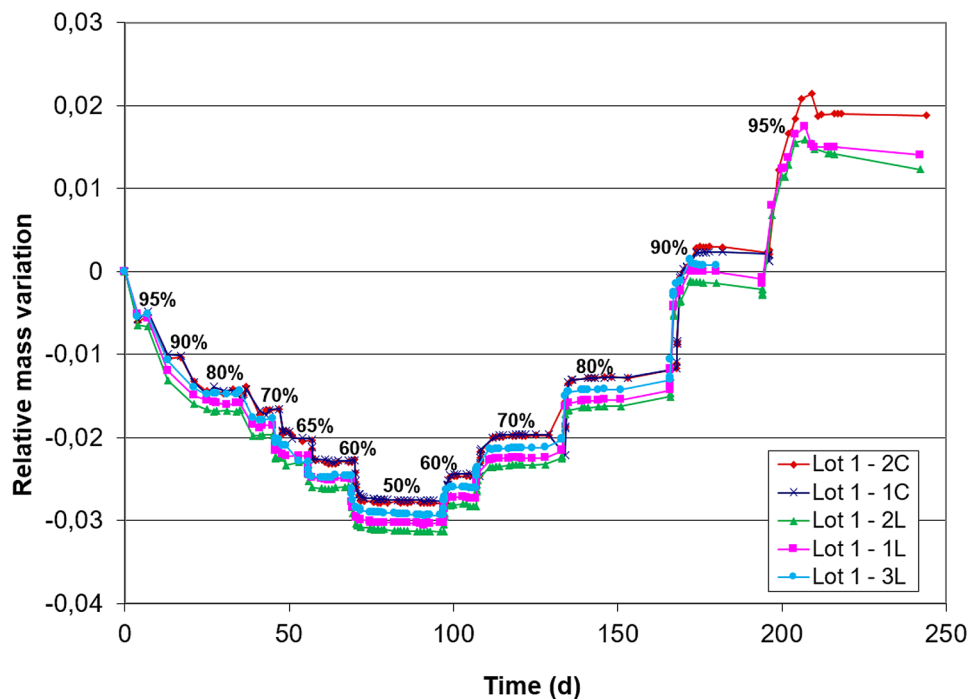


Fig. 3 Sketch-potential cracking induced by drying

Fig. 2 Mass variation of argillite sample submitted to drying then imbibition



(which are nevertheless present). Among structural causes, boundary constraints play also a significant role in desiccation crack initiation as they contribute to the occurrence of tensile stresses (Peron et al. 2005). These constraints act as an interface between drying and non-drying zones inside a sample (see Fig. 3). The tests, performed in this study, can be considered as free desiccation (or wetting) ones as no special device was used to externally prevent shrinkage (or swelling) of samples. Even if beyond the scope of this study and based on the previous comments, it is clear that cracking would strongly depend on the sample size and/or on the resulting drying/wetting kinetics linked to this size i.e. the necessary time to obtain an homogeneous sample saturation state. Hence, the produced damage is strongly dependent on the drying/wetting rate, which is linked to the moisture gradient in the sample. This has been clearly demonstrated by Wang (2014) in a study on the cracking (COx rock) produced by drying/wetting at a micrometric scale on thin samples (1 mm). 1  $\mu\text{m}$  width cracks were observed and mainly produced at the beginning of the drying/wetting process (i.e. when the moisture gradient is the highest). Both wetting and drying processes produced damage but this experimental study does not allow to evaluate which one is the most deleterious.

The rock anisotropy is likely to play a role in the material cracking due to hydric changes as, in a first step, the latter will induce heterogeneous strains. Like other clay rocks such as Opalinus Clay (Minardi et al. 2016; Favero et al. 2018), COx argillite is generally regarded as a transverse isotropic material (Zhang and Rothfuchs 2008; Zhang et al. 2019) for which the isotropic plane is the ‘in-situ’ bedding plane 1–2 (Fig. 4). Most of the permeability and mechanical tests further presented were performed according to case a. In parallel one series of permeability tests was carried out with a flow direction perpendicular to the bedding plane (case b).

The anisotropy of COx argillite was confirmed by recording the strain during wetting (or drying) of samples cored either along axis 1 (or 2) or axis 3 (Fig. 5). The results are summarized in Fig. 6 and put in light a strong strain anisotropy v.s. total suction (or relative humidity), which is around 3 (i.e.  $\epsilon_3/\epsilon_1 \approx 3$ ), which means that the shrinkage (or swelling) effect is much more pronounced along axis 3 (perpendicular to the bedding plane). Such a higher shrinkage (or swelling) perpendicular to the bedding plane was also detected on Opalinus clay (Minardi et al. 2016). Numerous results on COx argillite have also reported that Young modulus  $E_3$  is lower than  $E_1$  or  $E_2$ , however, with a ratio generally close to 2 (Zhang et al. 2012; Cariou et al. 2013).

Brazilian splitting tests were used to evaluate the tensile strength of the material for two cases that can underline that a bedding plane is a weakness plane (Fig. 7). The strength in case 1 was in the range of [0.8, 1.4 MPa] with always one distinct fracture parallel to the bedding plane. The strength

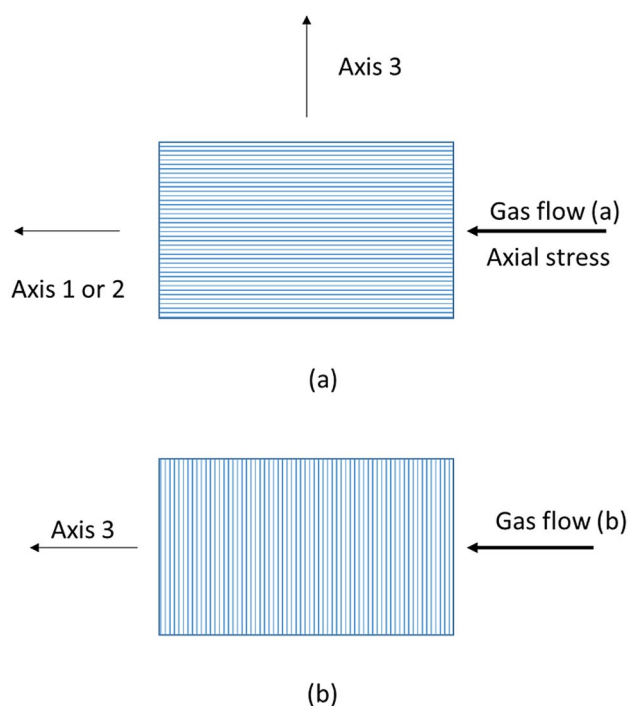


Fig. 4 Argillite anisotropy

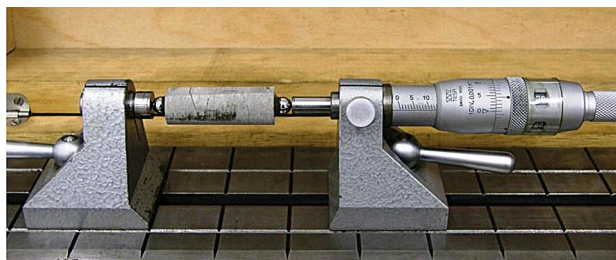


Fig. 5 Length variation measurements at a different level of relative humidity

value was in the range of [2, 4.5 MPa] for case 2 with sometimes multiple cracks and erratic orientations.

### 3.2 Reference State and Experimental Conditions

Gas permeability is very sensitive to cracking and to material water saturation level, for which it is called effective gas permeability. It will be observed in the following that argillite Young modulus is also very sensitive to the material’ water content.

Note as regards gas permeability: The occurrence of cracks obviously leads to an increase in gas permeability and a higher sensitivity to confining pressure. Previous results obtained on COx argillite are illustrated in Fig. 8. They clearly show that a higher initial value of

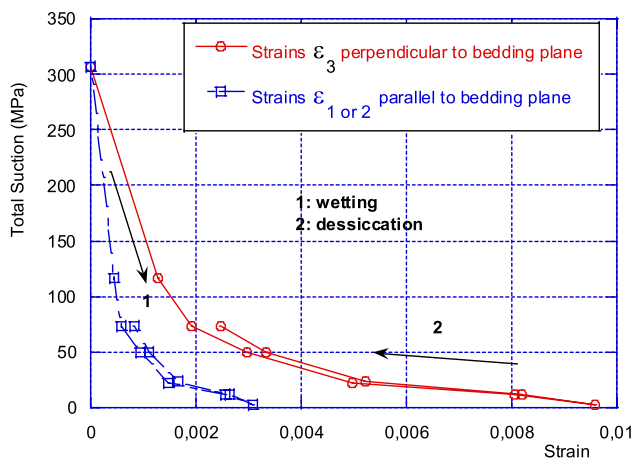


**Fig. 6** T-Cell 44564-Anisotropic strains due to wetting (or desiccation)

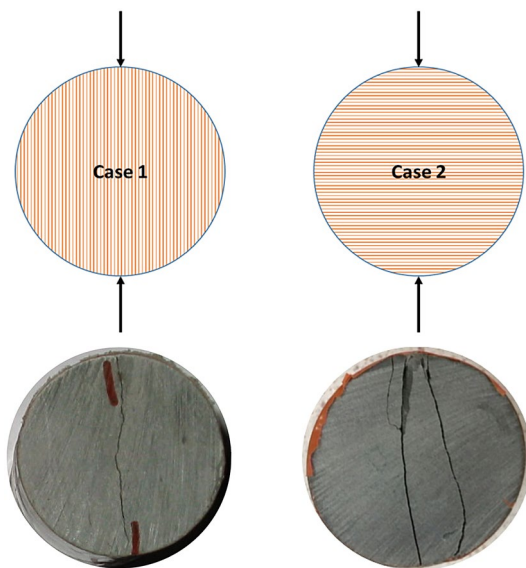


**Fig. 7** Brazilian tests: case 1 parallel to bedding plane—case 2 perpendicular to the bedding plane

permeability (i.e. more cracked sample) makes it more sensitive to confining pressure, which closes the cracks. Such a phenomenon was observed for concrete, mortar as well (Pei et al. 2017) and many other rocks (Wang et al. 2017; Zhang et al. 2020). It can therefore be admitted that concomitant increase in (gas) permeability and in confining pressure sensitivity is a powerful tool to evaluate the material damage (i.e. cracking). It is pointed out that the confining pressure effect is not reversible. This is linked to an irreversible crack closure and justifies further observations at a low confining pressure ( $P_c = 0.5$  MPa) apart from the last test that was conducted up to 12 MPa confining pressure.

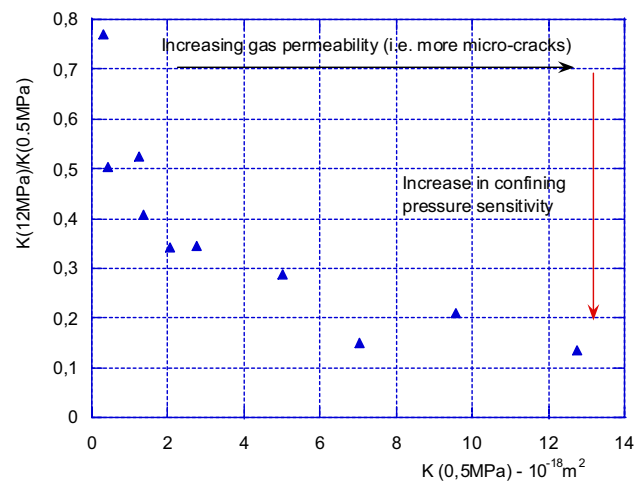


**Fig. 8** Variation of the permeability ratio  $K(12 \text{ MPa})/K(0.5 \text{ MPa})$  v.s. initial value  $K(0.5 \text{ MPa})$

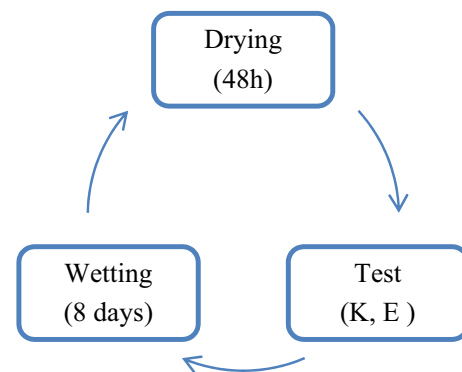


**Fig. 9** Wetting–drying cycles

A complete test for each sample is composed of successive cycles of drying and wetting (Fig. 9) especially at high RH levels (85% and more) and it had been chosen to analyze gas permeability and Young modulus variations at the only dried state (at 65 °C), which is assumed to be more objective to evidence the cracking. It is, in fact, long accepted that porous material saturation under humid cycles is strongly hysteretic (Davy et al. 2007; Song 2014; Zhang 2008). On the other hand, the RH cure level can be (quite easily) controlled since water saturation depends on the material tested. Some Young's modulus measurements on humid samples will be nevertheless presented.

Samples are first dried in an oven at 65 °C until constant mass. 2 days of drying revealed to be enough to assess stable drying. Based on previous tests (mentioned before) and on a complete pre-test presented below, 8 days were chosen for every step of wetting. Initial values of gas permeability ( $K$ ) and Young's modulus ( $E$ ) were measured after this first drying. Each sample was then put into a desiccator in which

the relative humidity is controlled with a brine solution. After 8 days sample was dried again at 65 °C to measure the resulting  $K$  and  $E$ . This kind of cycle was then repeated 3–4 times. Three levels of relative humidity RH 85%, 92% and 98% were favored as they are supposed to lead to more potential damage.

Note as regards the reference state: all the samples were tested at the dry state that was chosen as the reference one. Gas permeability and Young modulus depend not only on the crack network but also on the sample saturation level that reveals to be hysteretic, especially at high RH level. Hence the analysis of variations in these properties is more objective if conducted at the dry state. On the other hand, it is likely that both desiccation and wetting phases lead to material degradation (Yang et al. 2013). Testing the samples at the only dry state does not allow to deduce which phase is the most deleterious.

The permeability tests were carried out with the device described in Fig. 10. It is mainly composed of a hydrostatic cell to contain the sample. The tightness system is ensured with a (EPDM like Vitton) jacket. The cell and sample are connected to gas injection disposal. This gas device was designed in our laboratory and is able to measure gas permeability within the range ( $10^{-11}$  to  $10^{-22}$  m<sup>2</sup>). The techniques used to analyse and measure gas flow can be found with more details in (Song 2014). The confining pressure is controlled by a Gilson type pump. Gas permeability (for a cracked material) is very sensitive to confining pressure that leads to (partially) irreversible crack closure. It was therefore chosen to perform permeability test at a low confining pressure of 0.5 MPa to close the cracks as little as possible i.e. to better evidence damage. It would have been ideal to perform these tests without any confinement but it is mandatory due to tightness necessities. The injection pressure was fixed at 0.1 MPa, which is enough to detect gas flow through 10 mm sample thickness. It can be objected that such a low value is able to induce Klinkenberg effect (M'Jahad 2012; Didier 2012; Yuan 2017; Al Reda et al. 2020) leading to an apparent higher permeability than the intrinsic one. On the other hand, the same gas pressure was always used and,

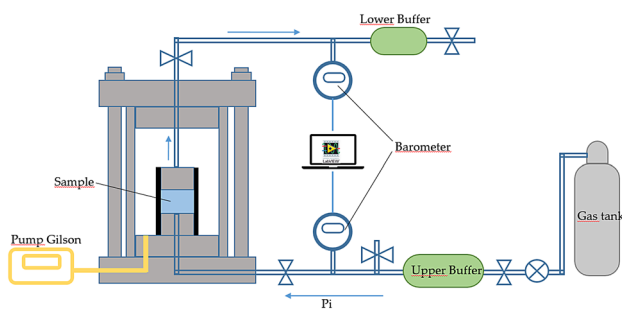


Fig. 10 Schematic diagram of the permeability test device

even if present, this effect will not affect the comparison of results obtained on the same sample. In the present case, it was chosen to deduce the permeability from the downstream flow rate  $Q_0$  (relation 1).

$$K = \mu \frac{Q_0}{A} \frac{2LP_0}{(P_i^2 - P_0^2)} \quad (1)$$

$\mu = 2.2 \cdot 10^{-5}$  Pa.s is the gas viscosity (pure argon),  $A$  is the sample cross-section area,  $L = 10$  mm its thickness,  $P_i = 0.2$  MPa absolute injection gas pressure and  $P_0$  is the atmospheric pressure at the free sample drainage side.

Young's modulus measurements were performed with a Zwick/Roell Z250 press. Strains were recorded and averaged from two 5 mm strain gages diametrically opposed at the sample center (Fig. 11). They were glued on the lateral sample surface after a complete surface preparation made up with a thin layer of epoxy resin. The Young modulus was extracted from the strain values obtained with an unloading step from 6 to 2 MPa axial stress. The loading and unloading rate was 0.01 mm/mn.

### 3.3 Sample Preparation and Pre-Tests

#### 3.3.1 Sample Preparation

ANDRA company had provided the laboratory with big cores called T-Cell from which smaller samples were cored. Argillite cylinders (37 or 20 mm diameter) were then cored and carefully cut into 10 or 40 mm lengths samples with a wire saw. Following this operation, they were preserved in sealed aluminum/plastic bags under vacuum

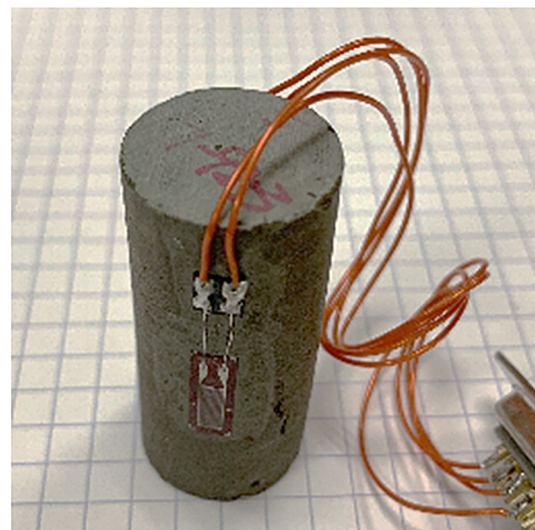
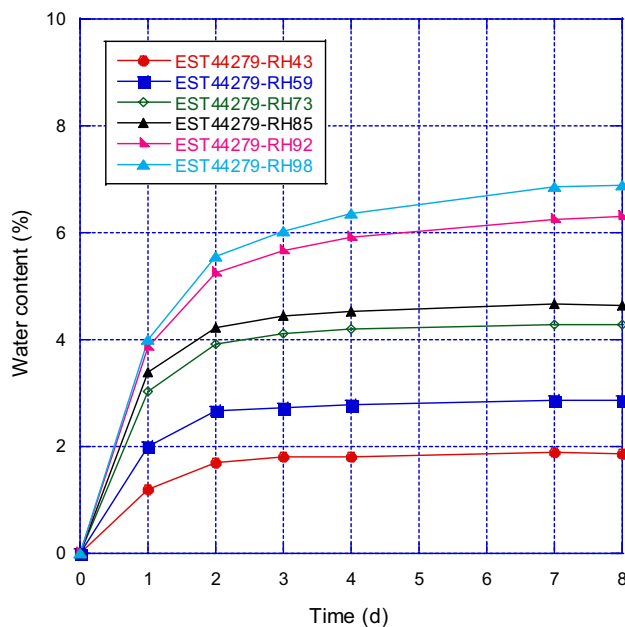


Fig. 11 Sample 20–40 for Young's modulus test

to avoid any risk of degradation due to change in their water saturation prior to be tested.

### 3.3.2 Water Saturation Pre-Test

All the pre-tests were conducted on the T-Cell EST44279 and performed according to case a, with the sample cylindrical axis parallel to bedding (see Fig. 4a). The main objective of this pre-test was to verify if the sample sizes were consistent with 8 days of wetting duration, which seemed to be a good compromise between the level of water saturation reached and the high risk of sample failure at 92 or 98% of RH after 10 days (and more) of wetting. 6 levels of RH (43, 59, 73, 85, 92 and 98%) were selected and the results on water content *w* v.s duration of wetting are given for 37–10 samples in Fig. 12. They clearly show that, after 1 day, most of the samples have already increase their water content by 50 to 70% of the final value. It is also to be noted that the mass equilibrium is almost reached from 7 days of wetting. On another hand, the comparison between 37–10 and 20–40 samples can be found in Table 1. Given the natural dispersion of such a material, the water contents at the lowest RH level (43–85%) are very close but there is a discrepancy at the highest levels (92 and 98%RH). Despite this fact, it was decided to maintain 8 days of wetting for both sample families (especially because over 8 days the rupture risk is too high under repeated cycles of wetting).



**Fig. 12** Evolution of water content in different saline solution environment

**Table 1** EST44279—Mass water content (%) in different saline solution environment after 8 days

W (%)	Samples 37–10	Samples 20–40
EST44279-RH43	1.85	2.11
EST44279-RH59	2.85	2.92
EST44279-RH73	4.28	4.34
EST44279-RH85	4.64	4.80
EST44279-RH92	6.32	5.40
EST44279-RH98	6.89	5.95

### 3.3.3 Permeability Pre-Test (Case a Flow Parallel to the Bedding Plane) and Selection of RH Levels

To minimize the total number of tests, it was necessary to work with a reduced number of relative humidity levels. They were selected through the gas permeability pre-tests results presented in Table 2. There is an increase in permeability for every cycle and RH level. However, the final one (after 3 cycles), which is given by the ratio ( $K_{end}/K_{init.}$ ), indicates that the highest RH levels lead to the strongest sample degradation due to cracking, which was expected. The sample EST44279-RH85 exhibits surprising results with a considerable increase in its permeability. This means that a strong cracking occurred for this sample (which in fact was close to rupture at the end of the cycles). However, such a degradation will not be met for the other series of samples cured at 85% of RH. It is also useful to observe the absolute increase in permeability  $\Delta K$  as, in a first approximation, it can be assumed to be caused by the cracks newly created i.e.  $\Delta K$  due to the “new crack network permeability”. This can give a rough order of magnitude of the cracks influence on permeability as the “new” crack network may also connect previous existing cracks, which were not connected before the cycles.

The samples were also submitted to permeability measurements under increasing confining pressure (see Table 3), which is generally supposed to close the cracks. The EST44279-RH85 one was not exploitable but the other results show that the sample sensitivity to confinement grows with the level of RH. This is highlighted with the ratio  $K_{12MPa}/K_{0.5MPa}$  that decreases with the level of RH. Being put together these results led to the choice of 3 RH levels for the whole set of following experiments: 85, 92 and 98%. They already indicate that the wetting/drying cycle repetition brings about a visible degradation of argillite samples. Other deductions can also be made from these results. Numerous permeability tests were performed on argillite on larger samples (generally 37 mm diameter and 70 mm height) and their gas permeability was often in the range  $10^{-17}$  to  $10^{-18} \text{ m}^2$  of the order of magnitude at 3–5 MPa initial confining pressure. In the present case, in which thinner

samples are used the initial permeability (at  $P_c = 0.5$  MPa) is in the range  $10^{-16}$  to  $10^{-17}$  m<sup>2</sup>. This can be due to a slight pre-cracking of the material, which effects on permeability are enhanced by the weak sample thickness. On the other hand, it can be observed that the confining pressure effect is quite spectacular. From 6 to 12 MPa, the usual level of permeability was almost recovered ( $10^{-18}$  m<sup>2</sup> order of magnitude) but, as it will be seen in the following, it was not observed for all materials (see results for samples EST44564 and EST48374).

## 4 Permeability Results

### 4.1 T-Cell EST 44564 (Flow Parallel to Bedding Plane—Case a)

Six 37–10 samples (RH85%, 92% and 98%) were machined to perform gas permeability measurements. The number of samples was doubled for the permeability tests as a kind of prevention in case of rupture. 3 complete cycles were performed for this second series. The results, presented in Table 4, are without any ambiguity: the wetting/drying cycles progressively increase the dry gas permeability. This

increase is clearly linked to the RH level used for the wetting cycles. The difference is spectacular after the RH98% cycles for which the degradation of permeability is almost 10 times higher than at RH85% (indicated with the ratio  $K_{end}/K_{init}$ ). The final values (cycle 3) for samples EST44564-RH85-2 and EST44564-RH92-1 can be considered as illogical as they are slightly lower than at cycle 2 but it probably just puts in light a lack of degradation between these two cycles. It is also useful to evaluate the absolute increase  $\Delta K$  in permeability showing that the EST44564-RH98 family exhibits a considerable permeability growing.

Figure 13 below plots the absolute-(a) and relative ( $K/K_0$ )-(b) gas permeability in dry state v.s. the number of wetting cycles. This representation is interesting as it shows that a large part of the degradation of samples EST44564-RH85 is obtained for the first cycle, there is no really significant evolution for the following cycles. This degradation is continuous for the EST44564-RH98 samples whereas the samples EST44564-RH92 are in an intermediate case.

The confining pressure effects, measured only after the last wetting/drying cycle, are given in Table 5 and graphically illustrated in Fig. 14. They show that 6 MPa confining pressure is generally enough for the samples to meet their initial permeability (i.e. initial dry state at

**Table 2** EST44279—gas permeability (m<sup>2</sup>) evolution with cycles of wetting/drying

Sample	Initial	1 cycle	2 cycles	3 cycles	$K_{end}/K_{init}$	$\Delta K$
EST44279-RH43	1.75E-17	2.04E-17	2.45E-17	3.03E-17	1.7	1.3E-17
EST44279-RH59	3.10E-17	3.31E-17	3.63E-17	6.80E-17	2.2	3.7E-17
EST44279-RH73	2.42E-17	6.89E-17	8.45E-17	1.09E-16	4.5	8.5E-17
EST44279-RH85	1.05E-16	1.29E-15	2.59E-15	4.92E-15	47.0	48E-16
EST44279-RH92	1.08E-16	6.36E-17	3.54E-16	1.09E-15	10.1	9E-16
EST44279-RH98	6.35E-17	7.41E-17	1.71E-16	6.57E-16	10.3	5.9E-16

**Table 3** EST44279—confining pressure effect on final gas permeability (m<sup>2</sup>)

$P_c$ (MPa)	0.5	3	6	9	12	$K_{(12)}/K_{(0.5)}$
EST44279-RH43	3.03E-17	1.23E-17	5.33E-18	3.31E-18	2.50E-18	0.083
EST44279-RH59	6.80E-17	1.55E-17	5.04E-18	2.96E-18	2.39E-18	0.035
EST44279-RH73	1.09E-16	6.13E-17	2.04E-17	9.49E-18	5.32E-18	0.049
EST44279-RH92	1.09E-15	2.16E-16	1.58E-16	4.25E-17	2.36E-17	0.022
EST44279-RH98	6.57E-16	4.30E-17	1.72E-17	8.37E-18	5.20E-18	0.008

**Table 4** EST44564—Gas permeability K(m<sup>2</sup>) results at dry state

Sample	Initial dry state	Dry state + 1C	Dry state + 2C	Dry state + 3C	$K_{end}/K_{init}$	$\Delta K$
EST44564-RH85-1	1.84E-16	3.94E-16	5.24E-16	6.91E-16	3.8	5.07E-16
EST44564-RH85-2	1.07E-16	4.82E-16	5.34E-16	4.89E-16	4.6	3.82E-16
EST44564-RH92-1	5.39E-17	4.11E-16	6.64E-16	6.38E-16	11.8	5.85E-16
EST44564-RH92-2	2.59E-17	1.05E-16	1.19E-16	1.81E-16	7.0	1.56E-16
EST44564-RH98-1	5.89E-17	2.16E-15	3.06E-15	3.95E-15	67.1	38.9E-16
EST44564-RH98-2	6.19E-17	4.51E-16	7.79E-16	1.58E-15	25.5	15.2E-16



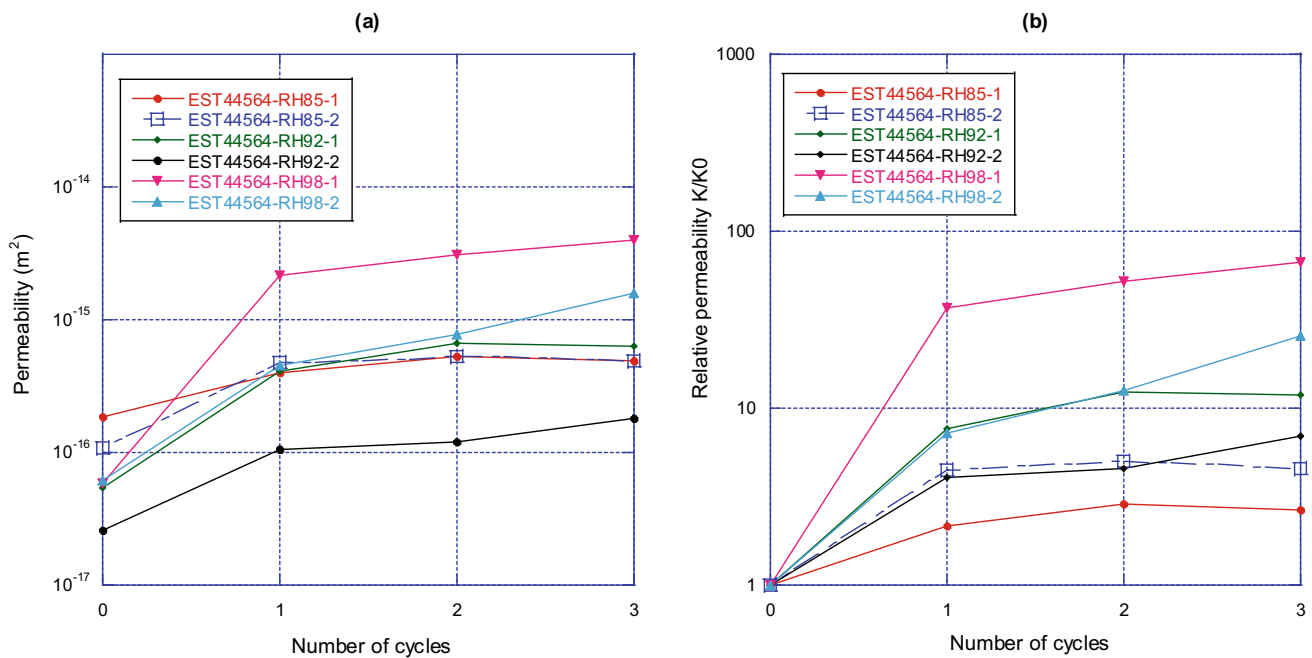


**Fig. 13** EST44564—Effective (a) and relative  $K/K_0$  (b) gas permeability in a dry state

**Table 5** EST44564—effect of confining pressure on gas permeability ( $m^2$ ) in dry state

$P_c$ (MPa)	0.5	3	6	9	12	$K_{12}/K_{0.5}$
EST44564-RH85-1	6.91E-16	2.45E-16	6.52E-17	3.80E-17	2.48E-17	0.035
EST44564-RH85-2	4.89E-16	1.17E-16	4.40E-17	2.28E-17	1.41E-17	0,028
EST44564-RH92-1	6.38E-16	8.62E-17	5.93E-17	3.68E-17	3.07E-17	0,048
EST44564-RH92-2	1.81E-16	9.93E-17	5.10E-17	3.24E-17	2.13E-17	0,117
EST44564-RH98-1	3.95E-15	2.45E-16	1.23E-16	6.81E-17	4.15E-17	0,011
EST44564-RH98-2	1.58E-15	4.70E-16	1.71E-16	9.31E-17	6.10E-17	0,038

0.5 MPa confining pressure) except for the EST44564-RH98 samples, which were obviously more degraded by the wetting cycles. For these two last ones, a pressure of 12 MPa is needed to be close to their starting permeability value. There is always a strong influence of the confinement but the final ratio ( $K_{12\text{MPa}}/K_{0.5\text{MPa}}$ ) seems to be less indicative than for the first pre-tests. It must be then taken into account that the confining pressure will close all the cracks i.e. the previous ones, already present before the sample testing and the one due to the wetting cycles. The increase in permeability (i.e. given by the ratio  $K_{\text{end}}/K_{\text{init}}$ , see Table 5) is more objective as it really gives the influence of the cracks newly created. The samples EST44564-RH85 were likely to be already damaged in their initial state as their permeability was higher than the one of the other samples. On another hand, this means that the confining pressure will also close this initial cracking, which is included in the ratio  $K_{12}/K_{0.5}$ .

#### 4.2 T-Cell EST 44564 (Flow Perpendicular to Bedding Plane—Case b)

As mentioned before in §3–1, CO<sub>x</sub> argillite is a transverse isotropic rock. This isotropy was clearly visible in Fig. 6 that indicated a strain ratio, due to wetting (or drying),  $\epsilon_3/\epsilon_1 \approx 3$ . The bedding plane was also found to be a weakness zone as regards the tensile strength measured with Brazilian tests. Enough material was available to core five more samples along axis 3 in T-Cell 44564 to evaluate the effect of hydric cycles on the gas flow (i.e. gas permeability  $K_T$ ) perpendicular to the bedding plane (case b of Fig. 4b). This allowed the comparison of the hydric cycle effects in two directions for the same core. Two levels of relative humidity were used as they are supposed to produce the most severe effects: RH92 and RH98%. The results are presented in Table 6 and Fig. 15. The last column in Table 6 is the ratio  $K_T(P_c = 12\text{MPa})/K_T(P_c = 0.5\text{MPa})$  obtained after the third hydric cycle.

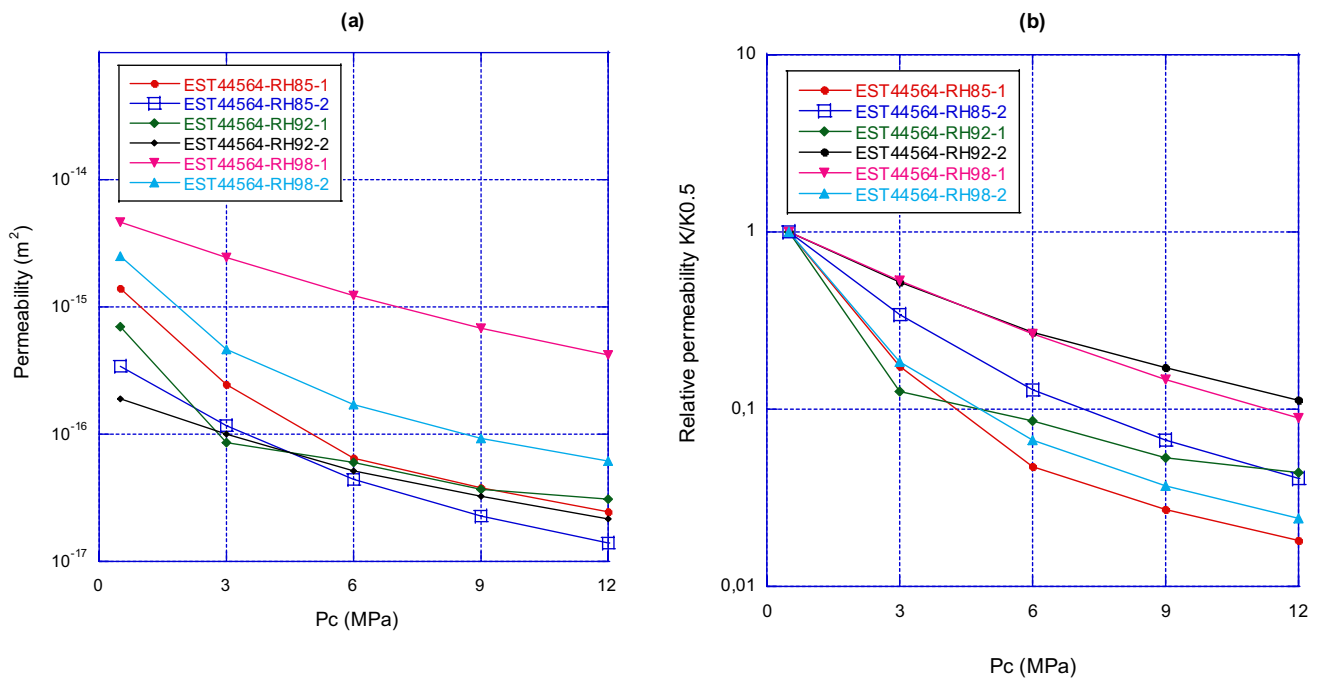
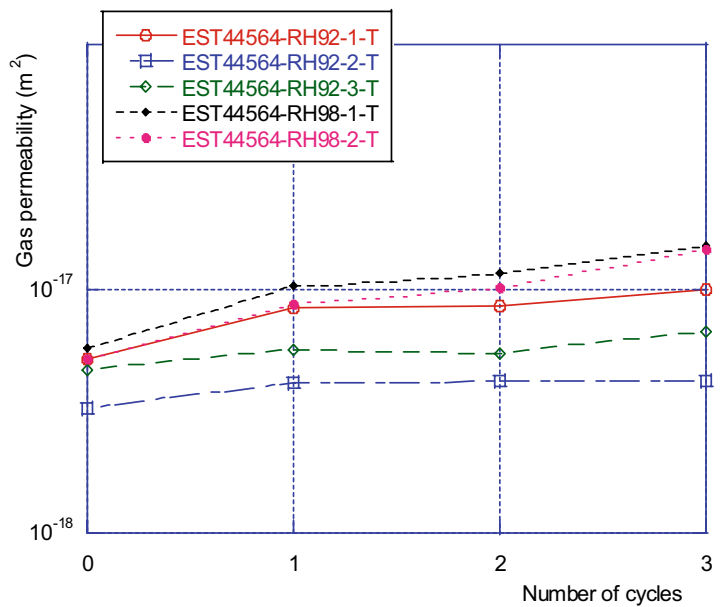


**Fig. 14** EST44564—Effect of confining pressure—absolute (a) and relative  $K/K_{0.5}$  (b) gas permeability in a dry state—flow parallel to the bedding plane

**Table 6** EST44564—gas permeability  $K_T(m^2)$  with a flow perpendicular to the bedding plane

Sample	Initial dry state	Dry state + 1C	Dry state + 2C	Dry state + 3C	$K_{Tend}/K_{Tinit}$	$K_{T12}/K_{T05}$
44564-RH92-1-T	5.14E-18	8.28E-18	8.48E-18	9.93E-18	1.93	0.18
44564-RH92-2-T	3.23E-18	4.14E-18	4.19E-18	4.18E-18	1.29	0.42
44564-RH92-3-T	4.66E-18	5.65E-18	5.47E-18	6.73E-18	1.45	0.36
44564-RH98-1-T	5.70E-18	1.02E-17	1.15E-17	1.51E-17	2.65	0.11
44564-RH98-2-T	5.16E-18	8.62E-18	1.02E-17	1.45E-17	2.81	0.17

**Fig. 15** EST44564—Effective gas permeability in a dry state



Despite the rock anisotropy, the ‘ $K_T$ ’ gas permeability is generally of the same order of magnitude as  $K$  ( $K$  is, in the following, the permeability measured parallel to the bedding plane) (Delay et al. 2006). This low gas permeability anisotropy was confirmed by many tests performed in LaMcube laboratory with a ratio  $K/K_T$  being often in the range [1, 2]. The comparison between the initial permeability values, however, shows that  $K_T$  is one order of magnitude less than  $K$ . Moreover, the successive hydric cycles obviously led to a higher relative increase in  $K$  than for  $K_T$ . The maximum relative increase, after three hydric cycles, is less than 3 for  $K_T$  since it can reach 67 (see Table 4) for  $K$ . The cycle effects are compared for both series of samples, in Fig. 16 in which the two families of results are clearly distinct. Such results demonstrate that the hydric cycles have a more pronounced impact on the ‘ $K$ ’ permeability than on the ‘ $K_T$ ’ one. This higher impact occurred from the first step of drying as indicated by the initial permeability values, and is amplified with the repeated cycles. The relative effect of confining pressure, evaluated with the ratio  $K_{12}/K_{05}$ , exhibits higher values for the ‘ $K_T$ ’ permeability than for the ‘ $K$ ’ one. This can be interpreted by a lower level of damage and crack opening. Even if lower, this damage led to an obvious change in permeability behaviour v.s. confining pressure  $P_c$ . This phenomenon is highlighted in Fig. 17, in which are compared the permeability for an intact sample (i.e. after the first drying) and sample 44564-RH98-2-T. Two points can be underlined: the relative effect of  $P_c$  and the irreversibility of permeability after unloading are more pronounced for the sample submitted to hydric cycles.

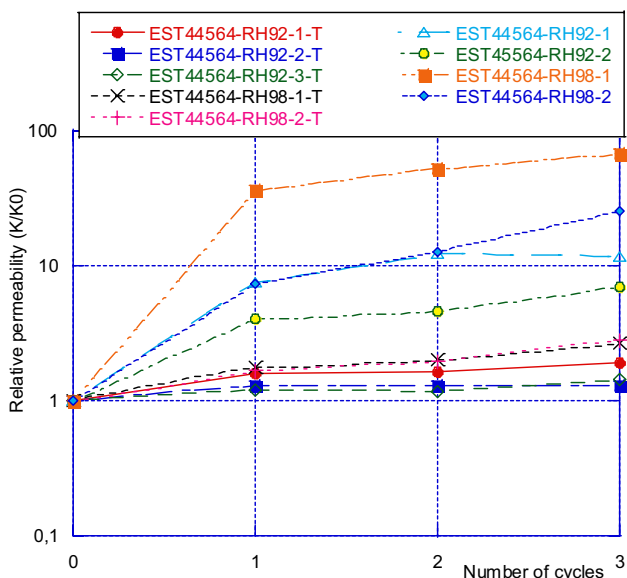


Fig. 16 EST44564- relative  $K/K_0$  gas permeability in dry state—samples \*-T are submitted to flow perpendicular to bedding

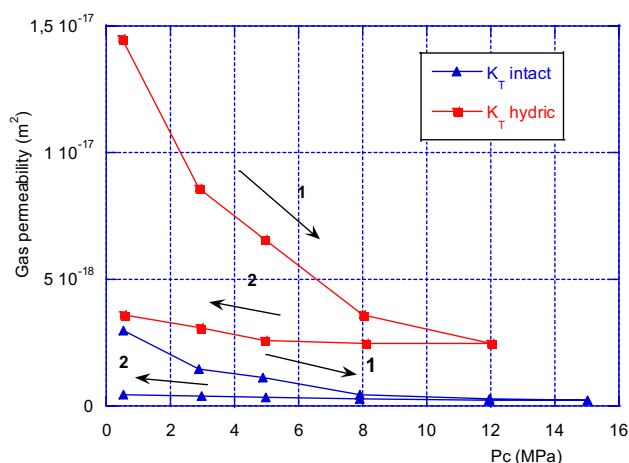
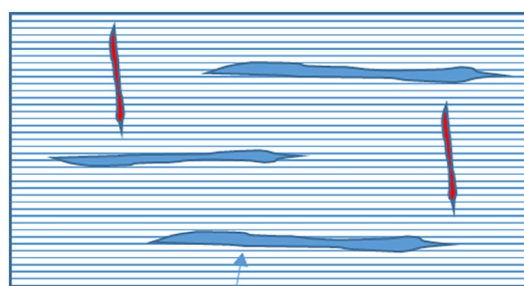


Fig. 17 Comparison of the sensitivity to confining pressure between an intact sample and a degraded sample—flow perpendicular to bedding plane—arrow 1 = first step—loading, arrow 2 = unloading

As a whole, these complementary results led to more visible damage in the bedding plane and hypothesis of cracks that are mainly located as drawn in Fig. 18. This scheme is consistent with the fact of bedding planes being a weakness zone for tensile stresses, which develop during structurally prevented shrinkage. This phenomenon has been confirmed in (Wang 2014) with the observation, at a micro-metric scale, of a majority of cracks along the bedding plane.

### 4.3 About the Klinkenberg Effect—EST44564

Even if taking into account this potential effect is not really necessary to analyze the detrimental results on argillite gas permeability, it was nevertheless interesting to evaluate if



Main crack network in the bedding plane

Fig. 18 Scheme of a potential crack network deduced from gas permeability experiments

**Table 7** Est44564—variation of gas permeability with injection pressure—6 MPa confinement

$P_i$ (MPa)	0.2	0.5	1	3
$K$ (m <sup>2</sup> )	4.40E-18	4.04E-18	3.77E-18	3.80E-18

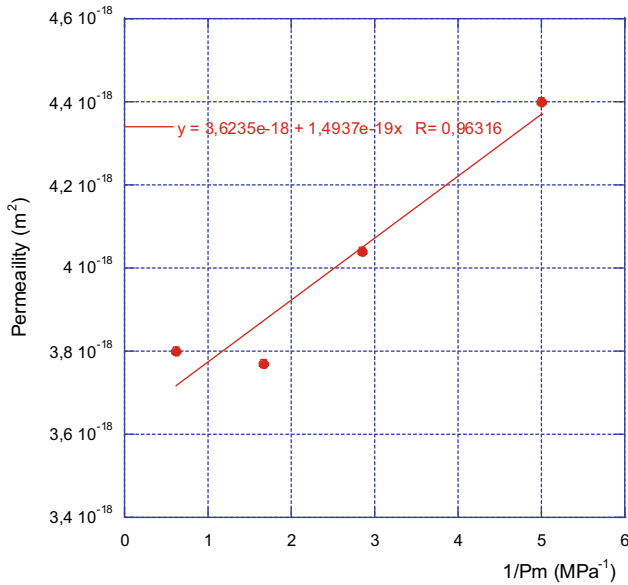


**Fig. 19** EST44564—Klinkenberg effect

this effect is present. It was done on one EST44564 sample, which is considered as ‘intact’ as just one drying was performed to measure its gas permeability. Table 7 below shows the results obtained at different injection pressure values and at 6 MPa confinement.

As it is well known, Klinkenberg proposed a very simple expression to take into account the slipping effect (Klinkenberg 1941):

$$K_{app} = K_{int} \left( 1 + \frac{b}{P_m} \right) \tag{2}$$

in which  $K_{app}$  is the permeability measured at different injection pressures,  $K_{int}$  is the intrinsic permeability,  $P_m$  is the mean pressure in the sample  $(P_{inj} + P_{atm})/2$  and  $b$  the Klinkenberg coefficient. It can be seen in relation (2) that the lowest injection pressure results in a higher apparent permeability. This relation matches quite well for the sample

tested (Fig. 19) but it also shows that the Klinkenberg effect can be considered as low since a value of  $3.7 \cdot 10^{-18} \text{ m}^2$  for the intrinsic permeability is obtained. On another hand, this test was performed at 6 MPa confining pressure on an intact sample 37–10. Its permeability, compared with the initial permeability values obtained on this series at 0.5 MPa confining pressure (see Table 5—“initial dry state” column), highlights the considerable effect of this pressure. This justifies the preference for a low confining pressure to evaluate the permeability degradation due to hydric cycles. After hydric damage, the results (see Table 7) clearly indicate that after hydric damage the degraded sample permeability does not meet the one of the non-degraded sample, even at 12 MPa confining pressure.

#### 4.4 T-Cell EST 48374 (Flow Parallel to Bedding Plane—Case a)

Three 37–10 samples (RH 85%, 92% and 98%) were machined for the gas permeability measurements. 2 cycles of wetting/drying were performed on this last series. The results are presented in Table 8. The EST48374-RH92 can be seen as atypical (or particularly resistant) as its permeability is almost not affected by the cycles. For this sample, it can be assumed that no additional cracking occurred during the test. The sample EST48374-RH98 shows less degradation than EST44564 but is finally comparable with what was observed for the first series (especially the  $\Delta K$  variation). The EST48374-RH85 sample seems to degrade more than for the previous series on a relative point of view ( $K_{end}/K_{init}$ ) but as a whole the  $\Delta K$  variation is comparable with those of the EST44564. In this last case, the degradation is comparable for samples EST48374-RH85 and EST48374-RH98.

The relative variation (v.s. number of cycles) is given in Fig. 20. It shows that a large part of degradation is obtained for the first cycle for the EST48374-RH85 sample whereas it is the second cycle that seems more deleterious for the EST48374-RH98.

The increase in confinement gave results presented in Table 9. Once again there is a strong effect of this loading on the different samples, especially for the EST48374-RH85 and the EST48374-RH98, which were more degraded by the wetting/drying cycles. It is clear that the EST48374-RH92 is ‘slightly’ cracked when compared to the other ones.

**Table 8** EST48374—gas permeability (m<sup>2</sup>) test results

Sample	Initial dry state	Dry state + 1C	Dry state + 2C	$K_{end}/K_{init}$	$\Delta K$
EST48374-RH85	9.42E-17	4.95E-16	6.98E-16	7.4	6.04E-16
EST48374-RH92	1.81E-16	1.96E-16	1.94E-16	1.1	0.13E-16
EST48374-RH98	2.69E-16	3.67E-16	1.01E-15	3.8	7.41E-16

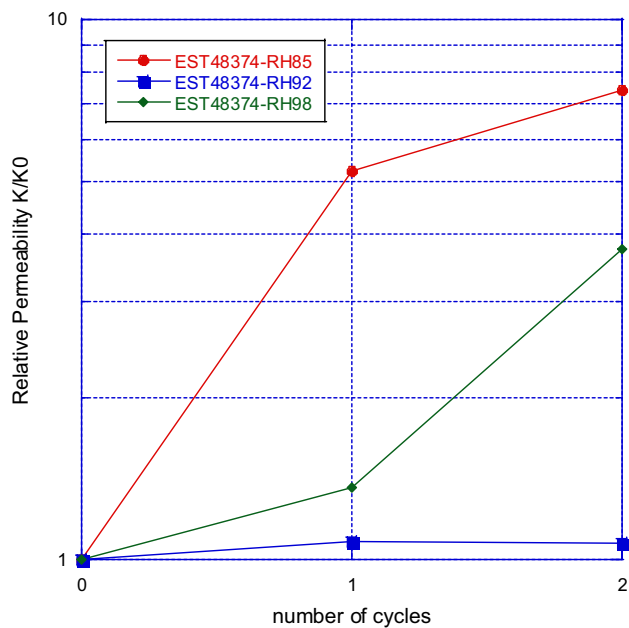


Fig. 20 EST48374—Relative variation  $K/K_0$  v.s. number of cycles

#### 4.5 Permeability Results Summary

Argillite is a natural material that exhibits a natural dispersion of its properties. As a consequence, the results obtained in this study must be analyzed as being able to indicate general tendencies. Numerous tests were previously performed in our lab (Davy et al. 2007; M'Jahad 2012; Yuan 2017) on dry argillite samples (with larger size) confined at 12 MPa confining pressure, which is supposed to be close to in situ stress conditions. Under such a high pressure, most of the tests gave gas permeability in the order of magnitude of  $10^{-18} \text{m}^2$  as it is indicated in Fig. 21. They were obtained for a flow parallel to bedding.  $K \approx 10^{-18} \text{m}^2$  is therefore chosen as being a reference material gas permeability value i.e. for 'intact' material at 12 MPa confining pressure. This 'intact material permeability' value is quite artificial as, to measure gas permeability, the material must be dried so perturbed. It can nevertheless be used for a purpose of evaluation of the effects of successive hydric cycles on gas permeability. On another hand, the present study focuses on gas permeability obtained at 0.5 MPa confining pressure and this point deserves some analysis to evaluate a possible value for

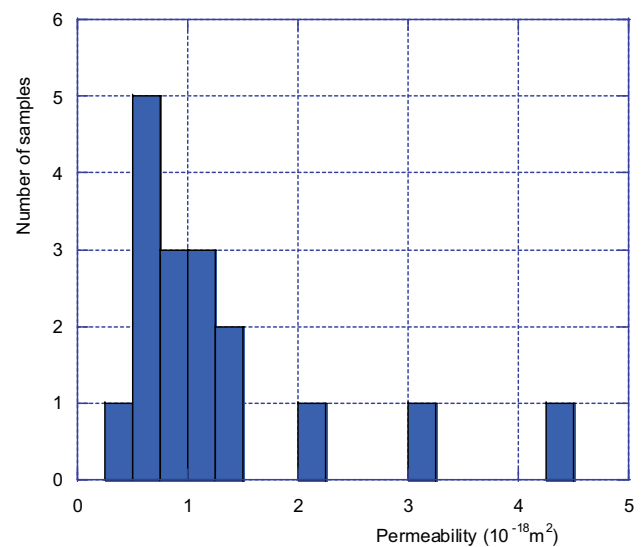


Fig. 21 Gas permeability measured at 12 MPa confining pressure in a dry state. Results obtained from previous studies on 17 samples. Mean permeability value is  $1.3 \cdot 10^{-18} \text{m}^2$ . Flow parallel to the bedding plane

the 'intact' permeability at this pressure, which remains unknown. Poromechanical experiments conducted on CO<sub>x</sub> argillite by Cariou et al. (2012) and Yuan (2017) showed that, despite the rock anisotropy, the Biot's tensor is isotropic with a Biot's coefficient value close to 1. It can then be deduced from this important result that the porosity variation  $\Delta\phi \approx \Delta\varepsilon_v$ , which is the volumetric strain due to a change in confining pressure  $\Delta P_c$ . From 0.5 to 12 MPa, the volumetric strain  $\Delta\varepsilon_v$  was experimentally found to be in the range  $[10^{-3}, 2 \cdot 10^{-3}]$ . As the CO<sub>x</sub> argillite porosity is around 18% the change in pore volume is in the order of magnitude of 1%. As a consequence and for a non-cracked porous material, the permeability variation due to the increase in confining pressure by 11.5 MPa should be low. For example, if the porous network is composed of cylindrical pores, such a change in pore volume leads to 0.5% decrease in pore radius and, assuming a laminar flow in these pores, this would induce a decrease in permeability by 2%. Such a simple calculation clearly shows that, for a non-cracked material (rock or concrete), the gas permeability will exhibit very little variation under confinement—except if the later induces pore collapse (soft chalk case for

Table 9 EST48374—gas permeability ( $\text{m}^2$ ) of effect of confining pressure

$P_c$ (MPa)	0.5	3	6	9	12	$K_{12}/K_{0.5}$
EST48374-RH85	6.98E-16	6.55E-17	4.86E-17	4.68E-17	4.72E-17	0.068
EST48374-RH92	1.94E-16	1.27E-16	5.60E-17	4.50E-17	4.33E-17	0.223
EST48374-RH98	1.01E-15	1.96E-16	1.21E-16	8.13E-17	6.54E-17	0.065

example). This means that if the material permeability is  $10^{-18} \text{m}^2$  under 12 MPa confining pressure then its permeability at 0.5 MPa will be slightly higher if the material is not cracked and not 10 (or more) times higher. It is why the assumption of an ‘intact’ material permeability of  $10^{-18} \text{m}^2$  seems reasonable. Another argument, able to strengthen this assumption, relates to the permeability anisotropy  $K/K_T$  that is weak at 12 MPa (between 1 and 2). The results, presented in Tables 4 and 6 (sample 44564), give a mean permeability  $K = 82 \cdot 10^{-18} \text{m}^2$  (flow parallel to bedding) and  $K_T = 4.8 \cdot 10^{-18} \text{m}^2$  (flow perpendicular to bedding) after the first drying. The anisotropy ratio is now  $K/K_T = 17$ . Such a high value is likely to be due to a large amount of cracks parallel to the bedding plane. Moreover, studies have reported a crack width of 1–5  $\mu\text{m}$  order of magnitude (Wang et al. 2014). A rapid and rough calculation assuming Poiseuille type flow through such a crack leads to an equivalent sample permeability of  $3 \cdot 10^{-16} \text{m}^2$  if there is one diametral crack through the whole 37–10 sample. Assuming Poiseuille law, the flow rate through the crack  $Q_c$  is given:

$$Q_c = \frac{ed^3}{12} \frac{\Delta P}{\mu L} \tag{3}$$

$d$  is the crack width (5  $\mu\text{m}$ ),  $e$  sample diameter (37 mm),  $\Delta P$  pressure difference,  $L$  sample length and  $\mu$  fluid viscosity.

In the non-cracked part, with  $A-(d.e) \approx A$ , the flow rate is:

$$Q_{nc} = AK_{nc} \frac{\Delta P}{\mu L} \tag{4}$$

$A$  is the sample section and  $K_{nc}$  the intact permeability supposed to be  $10^{-18} \text{m}^2$ . As the total flow rate through the sample is  $Q_c + Q_{nc} = Q$ , it can be obtained:

$$Q = K_{eq} A \frac{\Delta P}{\mu L} \text{ and } K_{eq} = K_{nc} + \frac{ed^3}{12A} \tag{5}$$

Using the geometrical test conditions it is thus obtained  $K_{eq} \approx 3 \cdot 10^{-16} \text{m}^2$ . It is interesting to observe that this value is consistent (on an order of magnitude point of view) with many results obtained after hydric cycles (see Tables 2, 4, 8).

It is therefore consistent to assume that the material can be significantly damaged after the first drying step. However, it cannot be assumed that this damage is only due to the drying as samples had undergone many potentially deleterious operations before the first drying step.

#### 4.5.1 Initial Permeability (i.e. After the First Drying and Before Hydric Cycles)

The initial permeability, carried out with a low confining pressure of 0.5 MPa (Tables 2, 6, 7) and a flow parallel to the bedding plane, was always found (i.e. for all the

samples) to be in the range  $10^{-16}$  to  $10^{-17} \text{m}^2$ . This is evidence that, even before any hydric cycle, the material had been modified and, in a first approach had been already cracked. This phenomenon is less visible when the flow is perpendicular to the bedding plane (Table 6) as the initial permeability is closed to the one supposed to be the intact one.

#### 4.5.2 Permeability Evolution Due to Hydric Cycles

The effect of hydric cycles is without any ambiguity linked, for every case, to an increase in gas permeability. Each cycle of wetting/drying induced a part of the final increase (excepted for one sample). As a result, it can be regarded as being an unavoidable phenomenon. Such an increase can be attributed to micro-cracking occurrence as, after having been submitted to hydric cycles, the gas permeability revealed to be very sensitive to confining pressure. This sensitivity can be represented in Fig. 22, which completes the Fig. 8. On the whole, there is a clear tendency: a higher increase in permeability leads to more sensitiveness to confining pressure. The zone of ‘intact’ material is related to a gas permeability lower than  $10^{-17} \text{m}^2$  while the ‘degraded’ zone is for the permeability recorded after the whole set of hydric cycles. The gas permeability was found to be in the range  $10^{-15}$  to  $10^{-16} \text{m}^2$ , which is two to three orders of magnitude more than what is likely to be representative of the matrix permeability (i.e. non cracked material). There was still an increase in permeability with a flow perpendicular to the bedding plane, but this increase was weaker. This obviously proves that any sample manipulation has to be carried out with extreme care to maintain the material close to its initial state and to be representative of in-situ material.

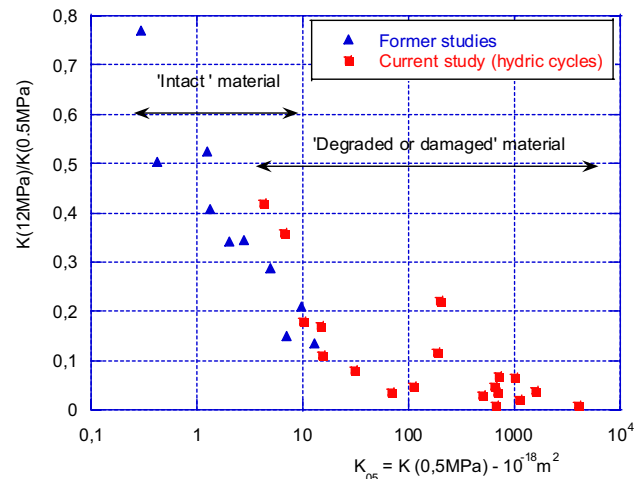


Fig. 22 Sensitivity of gas permeability to confining pressure v.s. permeability at 0.5 MPa. Complement of Fig. 8

## 5 Young's Modulus Measurements

### 5.1 T-Cell EST 44564 (Loading Parallel to Bedding Plane)

Four wetting/drying cycles were performed for this series of samples. They were loaded up to 6 MPa axial stress then unloaded for Young's modulus calculation. Such an unloading is necessary to record the elastic part of the axial strain. To evaluate the damage due to the cycles, it was chosen to compare the moduli for dry samples. It was nevertheless also interesting to obtain the Young modulus at the wet state. The results are given in Table 10. They are clear for the sample EST44564-RH85 as its moduli (at dry state) can be considered to be roughly constant (less than 5% decrease after 4 cycles). The decrease is close to 10% for the EST44564-RH92 sample and it had mainly occurred for the first two cycles. The EST44564-RH98 sample had (unfortunately) broken after the first cycle. The decrease obtained during this cycle was 15%, which is already a strong damage.

There is a considerable Young modulus decrease when the material is wet. The wet Young modulus is around two times less than the dry one. Even if frequently reported, this phenomenon reflects a strong structural modification of the material that can be put in parallel with the large swelling

at the highest humidity levels (Fig. 2). It is also clear that the (wet) Young modulus cannot be used to quantify the material damage.

### 5.2 T-Cell EST 48374 (Loading Parallel to Bedding Plane)

For this last series of test, 6 samples were submitted to 2 wetting/drying cycles. The results are presented in Table 11. Sample EST48374-RH85-2 excepted, the Young modulus of the other ones decreased by 7–20%. There is no strict rule as the decrease was either continuous (samples EST48374-RH85-1, EST48374-RH92-1) or occurred for the first cycle (EST48374-RH98-1, EST48374-RH98-2) or for the second one (EST48374-RH92-2). This is illustrated in Fig. 23 that plots the relative changes in Young modulus v.s. the number of cycles performed. This figure also shows that the most degraded sample is the EST48374-RH98-1 and the least is EST48374-RH85-2. The others (EST48374-RH85-1, EST48374-RH92-2, and EST48374-RH98-2) have the same Young's modulus relative decrease.

In Fig. 24 can be found the relative Young modulus variations that include the wet sample results. This clearly confirms the structural changes of argillite due to wetting.

**Table 10** EST44564—evolution of Young's modulus (GPa) related to water cycles

Sample	Initial dry state	Initial humid state	Dry state + 1C	Humid State + 1C	Dry state + 2C	Humid state + 2C	Dry state + 3C	Humid State + 3C	Dry state + 4C
EST 44564-RH85	<b>22.7</b>	9.79	<b>21.7</b>	10.3	<b>21.3</b>	11.4	<b>21.5</b>	10.4	<b>21.9</b>
EST44564-RH92	<b>21.9</b>	10.4	<b>21.3</b>	8.5	<b>20.3</b>	9.2	<b>20.2</b>	8.0	<b>19.9</b>
EST44564-RH98	<b>23.8</b>	10.0	<b>20.9</b>	7.0	–	–	–	–	–

Bold is used to highlight that the measurements were done in the dry state

**Table 11** EST48374—Young's modulus (GPa)

Sample	Initial dry state	Initial humid state	Dry state + 1C	Humid state + 1C	Dry state + 2C
Case	0	1	2	3	4
EST48374-RH85-1	<b>20.60</b>	12.30	<b>19.50</b>	10.80	<b>18.40</b>
EST48374-RH85-2	<b>23.60</b>	13.10	<b>23.40</b>	13.00	<b>23.50</b>
EST48374-RH92-1	<b>19.40</b>	11.20	<b>18.30</b>	10.50	<b>17.30</b>
EST48374-RH92-2	<b>20.70</b>	12.30	<b>20.30</b>	12.00	<b>19.30</b>
EST48374-RH98-1	<b>22.50</b>	10.20	<b>18.60</b>	9.20	<b>18.20</b>
EST48374-RH98-2	<b>23.80</b>	11.00	<b>21.90</b>	10.70	<b>21.60</b>

Bold is used to highlight that the measurements were done in the dry state

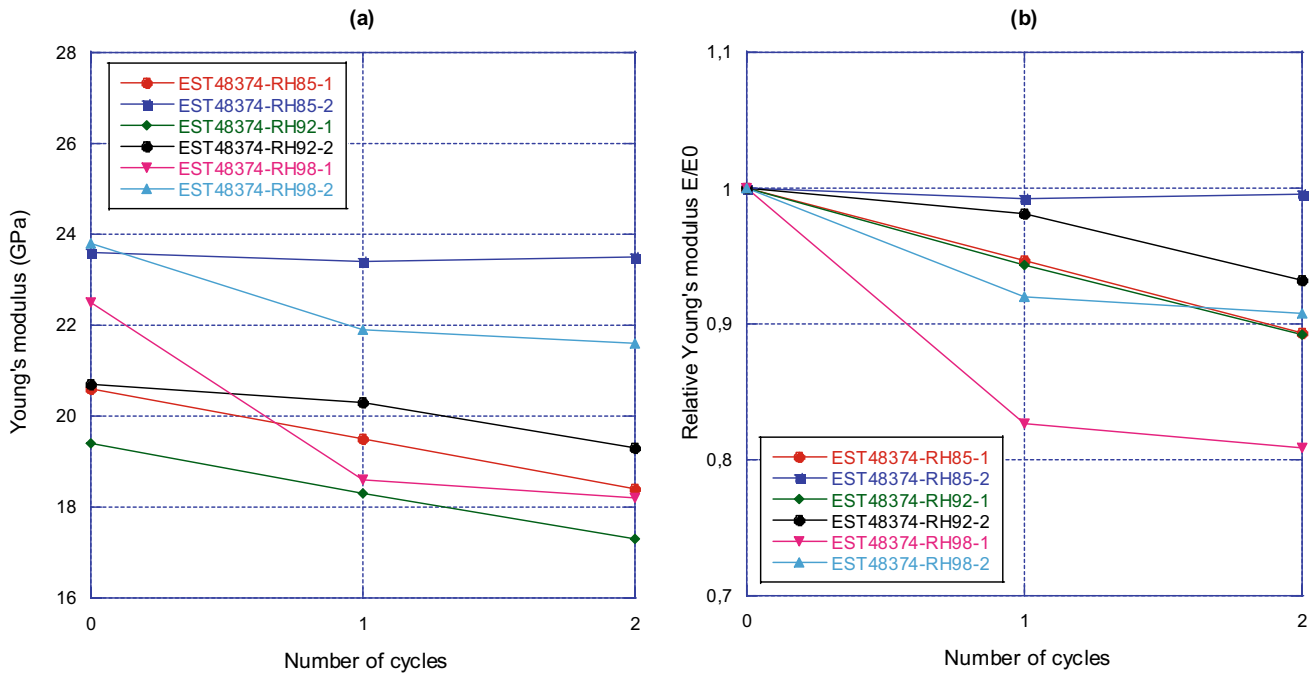


Fig. 23 EST48374—Effective (a) and relative (b) Young's modulus in dry state

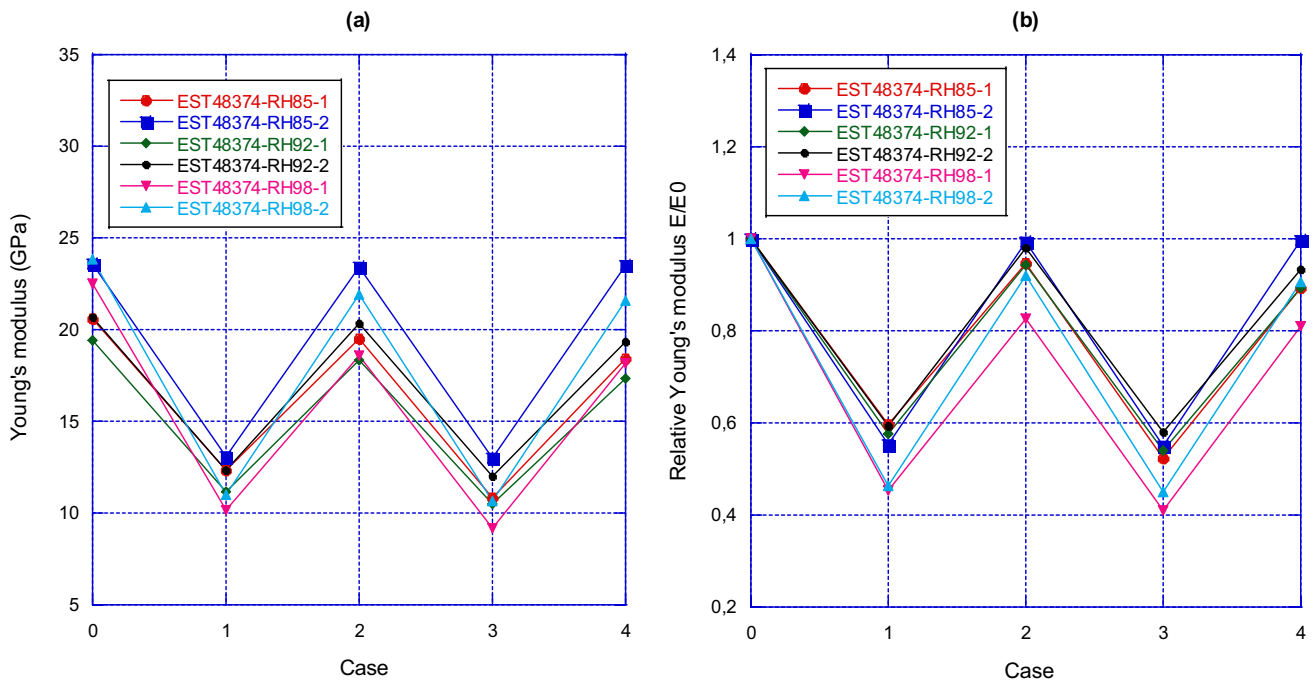


Fig. 24 EST48374—Effective (a) and relative (b) Young's modulus (cases 1 and 3: humid state)

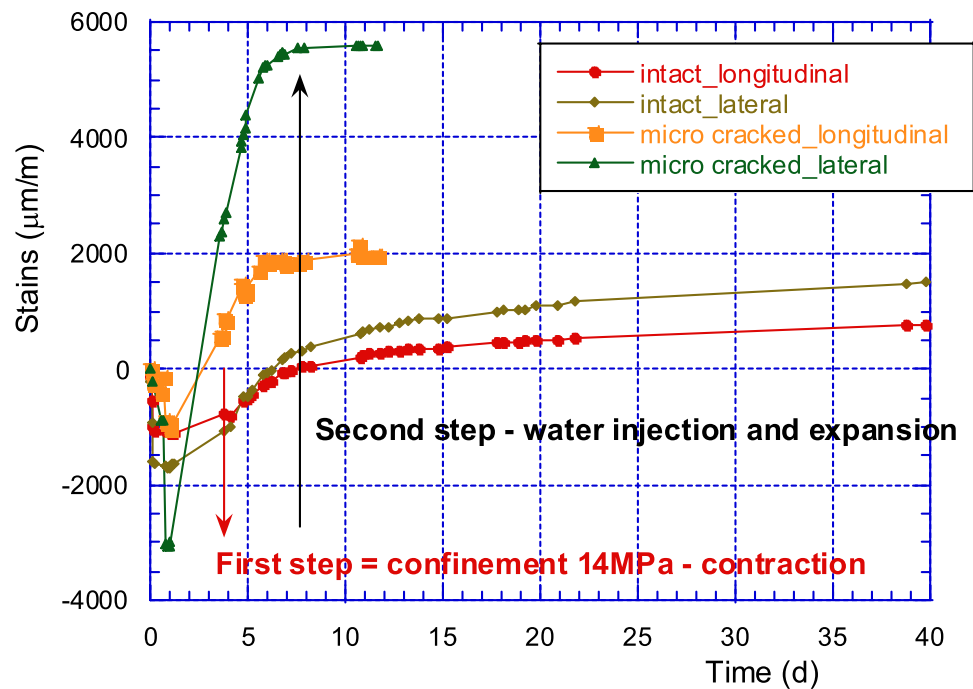
### 5.3 Young Modulus Results Summary

Even if it may be less spectacular than the variation in gas permeability, there is also a constant decrease in the Young modulus value due to hydric cycles. This decrease

can be interpreted as a sample damage, it is concluded that this is a confirmation of the sample micro-cracking. The dramatic decrease of this property, when measured on the wet sample, which has already been highlighted by many other experiments, indicates that the process of



**Fig. 25** Comparison of swelling for intact or micro cracked samples—first step confinement up to 14 MPa—second step synthetic water injection at 5 MPa on both sample sides—sample EST58145



water saturation is linked to a deep modification of the material's structure.

## 6 Discussion

The decrease observed in Young modulus is moderate as often less than 10%, which is of the same order of magnitude than the natural material dispersion. It must also be underlined that the Young modulus was measured along bedding plane axis that is 'a priori' less affected by damage than the Young modulus perpendicular to the bedding plane. In accordance with this observation, the use of gas permeability is clearly a better tool to evaluate the sample evolution due to hydric cycles and its degradation. This property exhibits a systematic increase and a sensitivity to confining pressure that can be favorably and simultaneously used to highlight the damage. Even if these experiments were conducted under quite extreme conditions, they clearly indicate that samples must be preserved close to their initial water saturation prior to being tested (in the case of the related test does not need dry or partially saturated state). Additional micro-cracking can in fact strongly modify many argillite properties: dry and effective gas permeability, compressibility, Young moduli and Poisson ratio, gas diffusivity, thermal expansion etc. On the other hand water permeability (always found in the range  $10^{-20}$  to  $10^{-21}$  m<sup>2</sup>), breakthrough pressure reveal to be very little affected by micro-cracking. This can be attributed to self-sealing properties of COx argillite.

Some interesting (and important) influence of cracking can also be found for swelling tests under confinement.

This kind of tests are currently performed in the LaMcube laboratory as they are necessary to investigate self-sealing properties of COx argillite or to evaluate Biot's coefficient values. Two samples, with a preserved initial water content of 7.5% (i.e. water saturation close to 90%), were tested under 14 MPa confinement (initial loading) then submitted to synthetic water injection (reconstituted water to be representative of the in-situ water) at a uniform pressure of 5 MPa. These 20–40 samples were instrumented like in Fig. 11 with two additional lateral gages to measure longitudinal (parallel to bedding) and lateral (perpendicular to bedding) strains. One of these two samples was initially damaged (cracked) with an axial compression test. The results of such an experiment are given in Fig. 25. It can be first underlined that, despite the high initial level of water saturation and an effective confinement of 9 MPa (Terzaghi effective confinement), the synthetic water injection leads to a global sample expansion. The presence of cracking induces three visible effects. Strains perpendicular to the bedding plane, due to the initial confinement, are higher for the cracked sample than for the intact one. This is consistent with the occurrence of cracks parallel to the bedding. The swelling kinetics is higher for the cracked sample than for the intact one, this can be due to the faster initial water imbibition due to cracks. Strong differences for the swelling amplitude can also be observed as the swelling of cracked sample is almost two times higher than the one of the intact sample. This effect can then lead to a significant impact on the swelling pressure evaluation, which can be chosen as being the pressure obtained during water imbibition under constant volume conditions.

## 7 Conclusion

Nuclear wastes are likely to be stored at Bure, in France, in underground facilities at great depth in a clay type host rock (COx argillite). As a consequence, this rock is (has been) intensively studied in laboratories as well as in the Bure underground laboratory. It is obvious that the laboratory tests must give representative rock properties, which will be met in-situ. It is clear that, among these properties, transfer and poro-mechanical ones are crucial and have to be accurately obtained. The main goal of this study was to evaluate the hydric cycle impacts (i.e. drying-wetting...) on gas permeability and Young modulus as both are very sensitive to micro-cracking. Several series of gas permeability tests and Young's modulus measurements were, therefore, carried out on argillite samples to evaluate the impacts of these cycles. Even if the tests were conducted under quite extreme conditions (repeated oven drying and wetting), they unambiguously indicate that the cycles result in additional micro-cracking, as a part of which may have been primary caused by coring or unconfinement for example. This cracking, which is amplified by the number of cycles, leads to a gas permeability that is likely to be much more higher than the non-cracked material permeability (possibly by one or two orders of magnitude) and to a decrease in Young modulus (parallel to bedding) by 5–15%. When measured with a flow parallel or perpendicular to the bedding plane, gas permeability was able to indicate and confirm that this plane can be considered as being a weak zone i.e. likely to be more easily cracked. Once again it is confirmed that gas permeability is a powerful and reliable cracking indicator, which allows sample selections (or rejection). In our opinion, the use of this property can be an efficient tool to evaluate and calibrate modelling of cracking due to drying/wetting or other stresses.

On another hand, such a study has led ANDRA to edit very strict rules on the water saturation state that must be preserved (water content higher than 7–7.5% i.e. water saturation of 90%) to avoid additional micro-cracking.

## References

- Al Reda SM, Yu C, Berthe G, Matray J-M (2020) Study of the permeability in the Opalinus clay series (Mont Terri—Switzerland) using the steady state method in Hassler cell. *J Pet Sci Eng* 184:106457
- Amann F, Wild KM, Loew S, Yong S, Thoeny R, Frank E (2017) Geomechanical behaviour of Opalinus Clay at multiple scales: results from Mont Terri rock laboratory (Switzerland). *Swiss J Geosci* 110:151–171
- Cariou S, Duan Z, Davy CA, Skoczylas F, Dormieux L (2012) Poro-mechanics of partially saturated COx argillite. *Appl Clay Sci Elsevier* 56:36–47
- Cariou S, Dormieux L, Skoczylas F (2013) An original constitutive law for Callovo-Oxfordian argillite, a two-scale double-porosity material. *Appl Clay Sci* 80–81:18–30
- Crisci E, Ferrari A, Giger SB, Laloui L (2019) Hydro-mechanical behaviour of shallow Opalinus Clay shale. *Eng Geol* 251:214–227
- Davy CA, Skoczylas F, Barnichon J-D, Lebon P (2007) Permeability of macro-cracked argillite under confinement: gas and water testing. *Phys Chem Earth Parts A/B/C* 32:667–680
- Davy CA, Skoczylas F, Lebon P, Dubois T (2009) Gas migration properties through a bentonite/argillite interface. *Appl Clay Sci* 42:639–648
- Davy CA, Skoczylas F, Talandier J (2013) Gas migration through COx claystone and implications for self-healing. In: *Poromechanics V*. American Society of Civil Engineers, Vienna. pp 1615–1624
- Delay J, Trouiller A, Lavanchy J-M (2006) Propriétés hydrodynamiques du Callovo-Oxfordien dans l'Est du bassin de Paris : comparaison des résultats obtenus selon différentes approches. *CR Geosci* 338:892–907
- Didier M (2012) Etude du transfert réactif de l'hydrogène au sein de l'argilite intacte. PhD dissertation, Université de Grenoble
- Favero V, Ferrari A, Laloui L (2018) Anisotropic behaviour of opalinus clay through consolidated and drained triaxial testing in saturated conditions. *Rock Mech Rock Eng* 51:1305–1319
- Freissmuth H (2002) Influence de l'eau sur le comportement mécanique des roches argileuses. PhD dissertation, Ecole Nationale Supérieure des Mines de Paris
- Klinkenberg LJ (1941) The permeability of porous media to liquids and gases, drilling and production practice. American Petroleum Institute, New York, pp 200–213
- M'Jahad S (2012) Impact de la fissuration sur les propriétés de rétention d'eau et de transport de gaz des géomatériaux : application au stockage géologique des déchets radioactifs. PhD dissertation, Ecole Centrale de Lille
- Marschall P, Horseman S, Gimmi T (2005) Characterisation of gas transport properties of the opalinus clay, a potential host rock formation for radioactive waste disposal. *Oil Gas Sci Technol Rev IFP* 60:121–139
- Minardi A, Crisci E, Ferrari A, Laloui L (2016) Anisotropic volumetric behaviour of Opalinus clay shale upon suction variation. *Géotechn Lett* 6(2):144–148
- Patriarche D, Michelot JL, Ledoux E, Savoye S (2004) Diffusion as the main process for mass transport in very low water content argillites: 1. Chloride as a natural tracer for mass transport-diffusion coefficient and concentration measurements in interstitial water: Chloride as a natural tracer for mass transport. *Water Resour Res* 40:W01516
- Pei Y, Agostini F, Skoczylas F (2017) The effects of high temperature heating on the gas permeability and porosity of a cementitious material. *Cem Concr Res* 95:141–151
- Peron H, Laloui L, Hueckel T (2005) Experimental evidence in desiccation cracking. Advanced experimental unsaturated soil mechanics, proceedings of conference, Trento, Italy, April 2005, 475–480
- Peron H, Delenne JY, Laloui L, El Youssoufi MS (2009) Discrete element modelling of drying shrinkage and cracking of soils. *Comput Geotech* 36:61–69
- Rutqvist J, Börgesson L, Chijimatsu M, Kobayashi A, Jing L, Nguyen TS, Noorishad J, Tsang C-F (2001) Thermohydromechanics of partially saturated geological media: governing equations and formulation of four finite element models. *Int J Rock Mech Min Sci* 38:105–127
- Song Y (2014) Water retention and fine microstructure of Bure argillite. PhD dissertation, Ecole Centrale de Lille
- Valès F (2008) Modes de déformation et d'endommagement de roches argileuses profondes sous sollicitations hydro-mécaniques. PhD dissertation, Ecole Polytechnique

- Wang LL, Bornert M, Héripré E, Yang DS, Chanchole S (2014) Irreversible deformation and damage in argillaceous rocks induced by wetting/drying. *J Appl Geophys* 107:108–118
- Wang L, Bornert M, Héripré E, Chanchole S, Pouya A, Bernard H (2015) Microscale insight into the influence of humidity on the mechanical behavior of mudstones: Hydromechanical behavior of mudstones. *J Geophys Res Solid Earth* 120:3173–3186
- Wang Y, Agostini F, Skoczylas F, Jeannin L, Portier E (2017) Experimental study of the gas permeability and bulk modulus of tight sandstone and changes in its pore structure. *Int J Rock Mech Min Sci* 91:203–209
- Wild KM, Wymann LP, Zimmer S, Thoeny R, Amann F (2015) Water retention characteristics and state-dependent mechanical and petro-physical properties of a clay shale. *Rock Mech Rock Eng* 48:427–439
- Wild KM, Barla M, Turinetti G, Amann F (2017) A multi-stage triaxial testing procedure for low permeable geomaterials applied to Opalinus Clay. *J Rock Mech Geotech Eng* 9:519–530
- Yang D, Bornert M, Chanchole S, Gharbi H, Valli P, Gatmiri B (2012) Dependence of elastic properties of argillaceous rocks on moisture content investigated with optical full-field strain measurement techniques. *Int J Rock Mech Min Sci* 53:45–55
- Yang D, Chanchole S, Valli P, Chen L (2013) Study of the anisotropic properties of argillite under moisture and mechanical loads. *Rock Mech Rock Eng* 46:247–257
- Yuan H (2017) Caractérisation expérimentale des propriétés de poromécaniques et de transfert de l'argilite du CO<sub>x</sub>. PhD dissertation, Ecole Centrale de Lille
- Zhang C (2014) Characterization of excavated claystone and claystone–bentonite mixtures as backfill/seal material. *Geol Soc Lond Spec Publ* 400:323–337
- Zhang C, Rothfuchs T (2004) Experimental study of the hydro-mechanical behaviour of the Callovo-Oxfordian argillite. *Appl Clay Sci* 26:325–336
- Zhang C, Rothfuchs T (2008) Damage and sealing of clay rocks detected by measurements of gas permeability. *Phys Chem Earth* 33:S363–S373
- Zhang F, Xie S, Hu D, Shao J, Gatmiri B (2012) Effect of water content and structural anisotropy on mechanical property of claystone. *Appl Clay Sci* 69:79–86
- Zhang N, Liu L, Hou D, He M, Liu Y (2014) Geomechanical and water vapor absorption characteristics of clay-bearing soft rocks at great depth. *Int J Min Sci Tech* 24:811–818
- Zhang C, Armand G, Conil N, Laurich B (2019) Investigation on anisotropy of mechanical properties of Callovo-Oxfordian claystone. *Eng Geol* 251:128–145
- Zhang D, Skoczylas F, Agostini F, Jeannin L (2020) Experimental investigation of gas transfer properties and stress coupling effects of salt rocks. *Rock Mech Rock Eng* 27:1
- Ziefle G, Matray J-M, Maßmann J, Möri A (2017) Coupled hydraulic-mechanical simulation of seasonally induced processes in the Mont Terri rock laboratory (Switzerland). *Swiss J Geosci* 110:195–212

**Publisher's Note** Springer Nature remains neutral with regard to jurisdictional claims in published maps and institutional affiliations.